Acta Cryst. (1979). A**35**, 181–188

The Structure of Ordered Ag_3Mg: an Ordinary Long-Period Alloy as Opposed to Periodically Antiphased Alloys

BY MICHEL GUYMONT

Laboratoire de Cristallographie et Physique des Matériaux, Bâtiment 490, *Université de Paris* XI, 91405 *Orsay CEDEX, France*

AND DENIS GRATIAS

Laboratoire de Metallurgie Structurale des Alliages Ordonnés, ENSCP, 11 *rue Pierre et Marie Curie,* 75231 *Paris CEDEX* 05, *France*

(*Received* 19 *April* 1978; *accepted* 18 *July* 1978)

Abstract

A necessary distinction is established between two kinds of long-period ordered structures: (1) periodic antiphases (PAP), whose principal characteristic feature is a continuous variation of antiphase half-period M as the composition changes; (2) 'ordinary' long-period structures, which show, as the composition changes, a series of phases stable in small composition ranges, every phase displaying a different, but well-defined, crystallographic structure. It is shown, through electron diffraction studies, that the ordered Ag_3Mg alloy belongs to the second kind, unlike standard PAP alloys such as AuCu, $AuCu_3$, Au_3Cu, Cu_3Pt and Cu_3Pd. It is stressed that standard PAP structures can always be obtained by heating, above some transition temperature, a $L1_2$ (or $L1_0$) phase which always exists at lower temperature. This is not the case for ordered Ag_3Mg. In this connection, the theory about stabilization of long-period structures is discussed [Sato & Toth (1965). *Alloying Behaviour and Effects in Concentrated Solid Solutions*, pp. 295–419. New York: Gordon & Breach].

Introduction

A number of alloys (AuCu, $AuCu_3$, Au_3Cu, Cu_3Pd, Au_3Zn, Ag_3Mg, Cu_3Pt *etc.*) display, in some ranges of concentration and temperature, particular structures known as periodic antiphases (PAP): the high-temperature disordered phase – generally of the $A1$ type – transforms to a low-temperature PAP structure, in one or two dimensions. Sometimes, at a lower temperature, an ordered $L1_2$ (or $L1_0$ in the case of AuCu) phase can be obtained which transforms itself into the PAP structure at a higher temperature. These experimental facts can be summarized by the transition scheme:

ordered $L1_2$ (or $L1_0$) → PAP → disordered $A1$,

when the temperature rises. This transition series is now well established for AuCu (Johannson & Linde, 1936), $AuCu_3$ (Pianelli, 1959), Au_3Cu (Gratias, Condat & Fayard, 1972), Cu_3Pt (Ogawa, Iwasaki & Terada, 1973) and Cu_3Pd (Guymont & Gratias, 1976).

The current literature does not make a clear distinction between such PAP structures and what we shall call 'ordinary' long-period structures. A PAP structure is one of the long-period structures, but PAP structures display characteristic features which enable them to be distinguished from among long-period structures. The clearest manner of discussing these characteristic features is to refer to the reciprocal space pattern as nearly displayed by electron diffraction. All alloys considered here are cubic in the $A1$ disordered phase and keep an orthogonal Bravais cell after transition: **a,b,c** the disordered cubic direct axes, and the

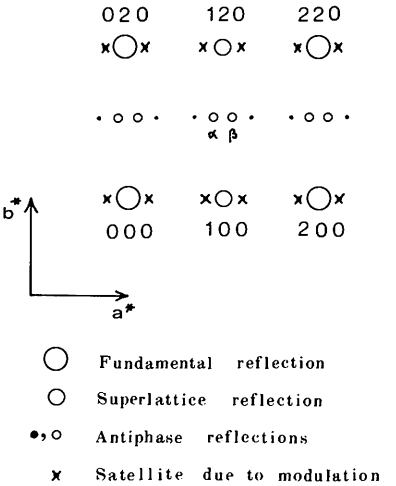

Fig. 1. Reciprocal plane (001)* for a PAP alloy. Only first- and second-order antiphase reflections are shown.

0567-7394/79/010181-08$01.00

reciprocal axes **a***,**b***,**c*** have the same direction. All through this study, all patterns will refer to these axes. We restrict our considerations to the case of the monoperiodic antiphase, and, for a clear discussion, we shall consider a unique orientation of antiphase direction in our drawings – as well as in our experimental observations.

The reciprocal plane (001)* is chosen with **a*** as the antiphase direction (Fig. 1): this drawing shows cell features common to all PAP alloys. The two antiphase reflections (or 'satellites') denoted α and β in the centre of this reciprocal {2**a***,2**b***,2**c***} cell have indices: α: $1-(1/2M)$, 1, 0; β: $1+(1/2M)$, 1, 0.

The distance $\alpha\beta$ is therefore $1/M$, in units of the reciprocal cell. M is, as usual, the antiphase half-period, and also represents the length of the antiphase domains in units of **a**.

Sometimes higher-order antiphase satellites are observed, the order being defined as $2n+1$ in the indices $1 \pm (2n+1)/2M$, 1, 0; however these become weaker as the order increases.

When concentration in the alloy is changed, the spacing between α and β varies, while all spots remain fairly sharp, which means that the antiphase long period is rigorously defined, although M seems to take any, in particular incommensurable, values.

This is the most striking characteristic feature of the PAP structure. For an ordinary structure, one can always choose a cell. This is not so in PAP structures: no cell can be chosen if M is not commensurable. Of course, 'giant' cells can be defined because the 'irrationality' of M can always be approached as close as is wanted with a rational number. But we think that such a description is devoid of physical meaning. As a consequence of the lacking of a cell, any description of PAP structures using space groups is impossible.

The proof of such an incommensurability has been given in AuCu II by X-ray studies on monocrystals (Jehanno & Pério, 1964; Jehanno, 1965): antiphase satellites have been observed up to the 7th order along the row of spots $X03$ and seem to overlap without superposition with projections on this row of higher-order satellites coming from the neighbouring 313 fundamental reflection.

A second feature of PAP structures is that experimental intensities of successive orders of antiphase reflections decrease more rapidly with order n than is predicted by the $1/(2n+1)^2$ law.† As intensities are not accurate in electron diffraction, which is the experimental tool used here, we shall not dwell any longer on this second feature.

On the other hand, structures with giant cells are known to exist, for instance in so-called non-stoichiometric oxides: unlike PAP, they are characterized by a discontinuous series of phases stable in small concentration ranges. We shall see that Ag_3Mg is another example of these latter structures.

Stability considerations

When it was recognized that most PAP alloys were equilibrium phases (Schubert, Kiefer, Wilkens & Haufler, 1955), the question of their stability was considered, *i.e.* why does a PAP structure form from the disordered $A1$ phase instead of the normal ordered (*e.g.* $L1_0$ or $L1_2$) phase?

The current theory of the formation of PAP – as well as of any long period – is due to Sato & Toth (1965). Using reasoning quite similar to that which Jones once used to discuss the relative stability of hexagonal close-packed and face-centred cubic structures of metals, they deduce a lowering of the Fermi energy due to the lengthening of the period. This reasoning is implicitly done at absolute zero, so that the lowering of energy for the PAP implies: $H_{PAP} < H_{ord}$, if H_{PAP} and H_{ord} denote the enthalpies of the PAP and of the normal ordered structure at 0 K.

In fact, this is not substantiated by the behaviour of AuCu, $AuCu_3$, Au_3Cu, Cu_3Pt and Cu_3Pd, for which there exists a $L1_2$ (or $L1_0$ for AuCu) phase at low temperatures. Hence, if this latter phase is in equilibrium, it can be stated that $H_{PAP} > H_{ord}$ (Guymont & Gratias, 1976).

All these alloys behave similarly when the concentration is varied and the previous discussion of the *Introduction* applies to them: they are true PAP alloys.

Ag_3Mg is reported to undergo a transition:

$$Ag_3Mg\ (A1) \rightarrow Ag_3Mg\ \text{(monoperiodic PAP)}$$

when the temperature is lowered in the range of composition from 20 to about 28 at.% Mg (Schubert, Kiefer, Wilkens & Haufler, 1955; Fujiwara, Hirabayashi, Watanabe & Ogawa, 1958). So far, no $A1 \rightarrow L1_2$ transition has been reported, which could well be for kinetic reasons. Our attempt to obtain a $L1_2$ phase for Ag_3Mg was without any success, and a detailed study has led us to a re-evaluation of the structure.

Experimental procedures

(1) *Ingot preparation*

The preparation of ingots of Ag_3Mg of known composition is not an easy matter for two principal reasons:

† There are other data about satellite intensities, but these do not seem to be characteristic of PAP. Antiphase satellites of the same order do not have the same intensity, this dissymmetry varying in a complex manner with composition, with the order of the reflection and also with X along the row of spots $Xk0$ considered. This also holds for 'satellites' of fundamental reflections: these can be due to multiple diffraction and/or modulation of atomic positions and/or modulation associated with the departure from stoichiometry (Ogawa, Watanabe, Watanabe & Komoda, 1958; Glossop & Pashley, 1959; Pério & Tournarie, 1959*b*; Jehanno & Pério, 1964).

(i) Mg is volatile: at 750°C its vapour pressure is 10 mm Hg.

(ii) Mg reduces silica (as it reduces most oxides). The only usual materials compatible with Mg at high temperatures are iron and graphite. The latter was preferred.

Pure Ag and Mg in known proportions were introduced into a graphite crucible hung in a vertical oven under one atmosphere of argon circulated for two days on a Ti–Zr alloy heated at 800°C. The ingot is then formed by heating at 960°C (melting temperature of pure Ag). At this temperature, the vapour pressure of Mg is about 200 mm Hg, resulting in an inevitable loss of Mg, and chemical analysis proved necessary.

The ingot obtained was turned over and remelted under the same conditions, thus preventing any segregation due to gravity. The metallic brightness of the final ingot is a warrant of minimal oxidation.

The ingots are rolled into thin strips about 0·1 mm thick and samples were cut from them. Several samples were then chemically analysed.

(2) *Quenching and annealing*

Samples were heated under one atmosphere of argon to 750°C for controlled times: 1, 5, 10 and 15 min. Thus the loss in Mg was gradual. Then, after quenching, several annealings were performed during times ranging from a few days to one month. Up to 400°C, annealing can be achieved in standard vacuum-sealed pyrex tubes.

(3) *Experimental observations*

Some of the annealed samples were used to make Debye–Scherrer diffraction patterns (Philips 114·6 mm diameter camera; Co $K\alpha$ radiation). Others were electrolytically thinned by the jet method using a Struers C_1 bath, and observed in transmission electron microscopy (Philips EM 300 microscope, with tilting device, operated at 100 kV).

(4) *Alloy compositions*

Chemical analyses performed show significant changes in composition of the ingots after the second melting. Differences are smaller, of course, between samples before and after quenching.

The accuracy of chemical analysis is not very high: not better than about 0·5 at.% Mg.

Fujiwara, Hirabayashi, Watanabe & Ogawa (1958) have published a plot of the crystal parameter of disordered α-Ag_3Mg against concentration. We have also used this curve to check our alloy concentrations. But the accuracy of this plot is poor and we have no reason to trust these measures of concentration more than ours.

The compositions of our samples were: 25, 24, 23·5 and 22 at.% Mg.

Reported ordered structure of Ag_3Mg

From 20 to about 22 at.% Mg, the antiphase half-period $M = 2$ is constant. The structure is then of the DO_{23} type (Fujiwara, Hirabayashi, Watanabe & Ogawa, 1958; Vanderschaeve, 1969) (Figs. 2 and 3). From X-ray experiments, some authors assume the DO_{23} structure in the whole range of composition 20–28 at.% Mg (Gangulee & Bever, 1968). Other studies, using X-ray powder diffraction (Schubert, Kiefer, Wilkens & Haufler, 1955) or electron diffraction on evaporated thin-film specimens (Fujiwara,

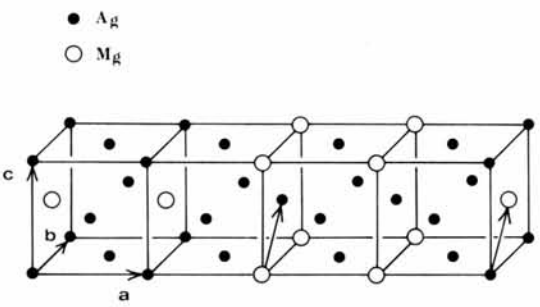

Fig. 2. The DO_{23} structure.

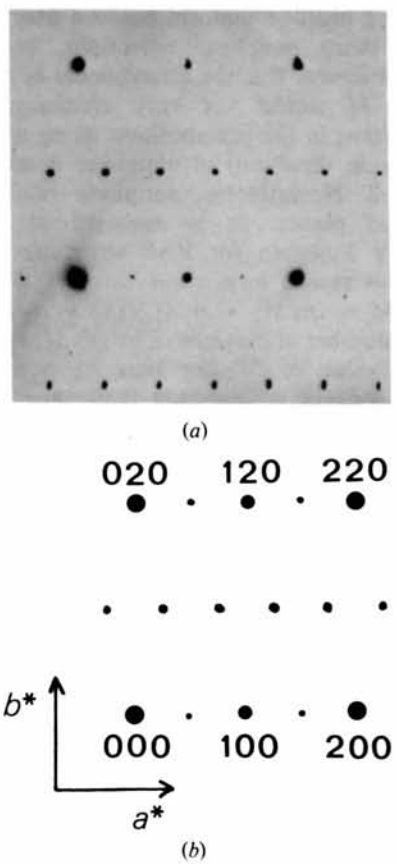

Fig. 3. (*a*) Diffraction pattern of an Ag–22 at.% Mg alloy quenched from 750°C and annealed at 320°C for 3 d: DO_{23} structure. All spots are equispaced. (*b*) Corresponding drawing.

Hirabayashi, Watanabe & Ogawa, 1958) or on bulk samples (Hahni, Mäki & Paalassalo, 1971) conclude that M decreases continuously from 2 to about 1·67 when the concentration varies from 22 to 28 at.% Mg. Usually, M is estimated from the spacing of the strongest satellite pair identified with the first-order antiphase reflections α and β. Indeed, the first measurements of M were carried out on X-ray powder patterns (Schubert, Kiefer, Wilkens & Haufler, 1955): it is unlikely that any but the strongest satellites were observed. Such a determination of M from powder patterns is much less accurate than the measurement carried out on electron diffraction patterns – or, equivalently, on X-ray diffraction patterns from monocrystals – where whole reciprocal planes are seen. All published electron diffraction patterns show two or three orientations for the antiphase direction, which does not help with the analysis.

The structure of Ag_3Mg between 22 and 28 at.% Mg is analysed by these authors (Fujiwara, Hirabayashi, Watanabe & Ogawa, 1958; Hahni, Mäki & Paalassalo, 1971) in terms of Fujiwara's model for PAP structures (Fujiwara, 1957). The continuously varying half-period M is accounted for by an average on antiphase domains of two different lengths ($M = 1$ and $M = 2$). This mixing must be uniform because only uniformity leads to sharp antiphase reflections, as these are actually observed. But the arrangement is not regular, otherwise M would not vary continuously: some disorder exists in the juxtaposition along **a** (chosen as the antiphase direction) of antiphase domains $M = 1$ and $M = 2$. Nevertheless, antiphase boundaries are well-defined planes, as is assumed in all models devised by Fujiwara for PAP structures (Fujiwara, 1957). This results in a mean value $\bar{M}$ computed as follows: $\bar{M} = (n_1 M_1 + n_2 M_2)/(n_1 + n_2)$, n_1 and n_2 being the number of domains of length M_1 and M_2. Any observed value of M can thus be accounted for. Finally, no exact arrangement is proposed, except of course, for $\bar{M} = 2$.

Pério & Tournarie's (1959*a*) model allows irrational values for M without referring to any mixing of integral cells and leads to the same values for calculated amplitudes.

Our conclusions are different: experimental results are quite well accounted for by Fujiwara's model of a 'regular arrangement with uniform mixing.'

Results

Our first experimental result is negative: we have never been able to obtain an ordered $L1_2$ phase.

Compositions between 20 and 22 at.% Mg give electron diffraction patterns such as the one represented on Fig. 3: it agrees well with the defined structure DO_{23}, which is an ordinary long-period structure of space group $I4/mmm$.

For compositions inside the range 22–26 at.% Mg and at several annealing temperatures, one observes the diffraction patterns given in Figs. 4, 5 and 6. These diffraction patterns are insensitive to the annealing temperature – at least for temperatures not greater than the disordering temperatures.

Fig. 7 is a dark-field micrograph corresponding to the pattern of Fig. 4 (25 at.% Mg, annealed at 345 °C for two days): the fringe structure along [100] is well developed. By comparison with a compound of known long period, we obtain an interfringe distance of 28 Å.

Turning to a close examination of the three diffraction patterns (Figs. 4, 5 and 6) we see that they correspond to three different structures. When compared to the standard diffraction pattern of any (monoperiodic) PAP alloy (Fig. 1), the main difference between Ag_3Mg and standard PAP (*e.g.* $AuCu_3$) patterns is the weaker spots inside the main 'satellites'. This contrasts with the monotonic variation in $1/(2n + 1)^2$. The three reciprocal rows of spots $X10$ are represented separately

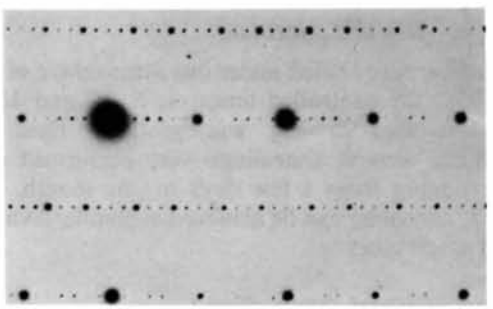

Fig. 4. Diffraction pattern of an Ag_3Mg alloy of about 25 at.% Mg quenched from 750 °C and annealed at 345 °C for 2 d.

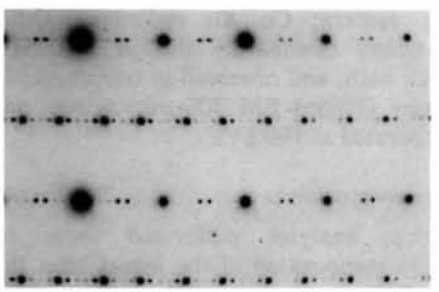

Fig. 5. Diffraction pattern of an Ag_3Mg alloy of about 24 at.% Mg quenched from 750 °C and annealed at 332 °C for 3 d.

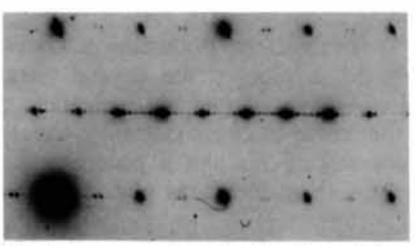

Fig. 6. Diffraction pattern of an Ag_3Mg alloy of about 23·5 at.% Mg quenched from 750 °C and annealed at 250 °C for 3 d.

for clarity (Fig. 8) where the spots are indexed in units of the reciprocal disordered cell. Further, we note:

(i) All spots are regularly spaced at submultiples of **a***. Therefore we can always choose a cell which retains **b** and **c** of the disordered cell and with a multiple of **a** in the third direction.

(ii) Superlattice spots $1k0$ with k even are not split in all three diffraction patterns (Figs. 4, 5 and 6). This implies that only $(\mathbf{b} + \mathbf{c})/2$ shifts are allowed. Hence, the splittings being along **a*** (see i), the antiphase vector is inside the antiphase plane (antiphase vector of the first kind).

(iii) For the row of spots $X10$ corresponding to the pattern of Fig. 4 (Fig. 8*a*) there is one spot 010 and the period is **a***/7 with a spot at each step. The period length is therefore seven disordered cells along the **a** axis. We thus have no lattice extinction and the Bravais lattice is P.

For the rows of spots $X10$ corresponding to the patterns of Figs. 5 and 6 (see Fig. 8*b* and *c*) there is no spot of indices 010: the first spot is $\frac{1}{18}$,1,0 for the row (*b*), hence a period of 18 disordered cells, but with a lattice extinction: no spot $n/18,1,0$ with n even. This leads to an I Bravais lattice. The same scheme applied to the row (*c*) also gives an I Bravais lattice and a period of 26 disordered cells along the **a** axis. This is also true for the DO_{23} structure (Fig. 3): here we obtain an I Bravais lattice with a period of four disordered cells along the **a** axis.

Any model suitable for the description of PAP structures is able to explain all these observed structures (Fujiwara, 1957; Pério & Tournarie, 1959*a*; Jehanno & Pério, 1964; Jehanno, 1965): all the weak spots observed between α and β first-order antiphase reflections are obtained as a superposition of successive higher-order antiphase reflections, which enhances the intensity of these spots, whilst in standard PAP diffraction patterns higher-order antiphase reflections vanish rapidly with the order: there is no enhancement by superposition of still higher-order antiphase spots. In other words, for PAP structures such as AuCu, $AuCu_3$, Cu_3Pd *etc.* we obtain an enumerable infinity of reflections in each reciprocal cell, whilst retaining the general aspect of the pattern: no spot will 'fall' on another spot whatever its order may be (Pério & Tournarie, 1959*a*). We think that in the case of Ag_3Mg, the antiphase half-period M does not vary continuously, because we have never obtained a diffraction pattern similar to that of standard PAP, but on the contrary, all patterns obtained can be explained by an ordinary, reasonable supercell.

We shall now discuss a model describing these structures.

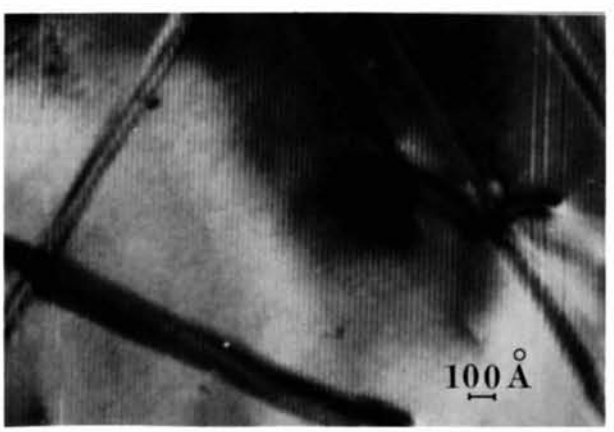

Fig. 7. Dark-field micrograph corresponding to diffraction pattern of Fig. 4 (25 at.% Mg sample). Interfringe distance: 28 Å.

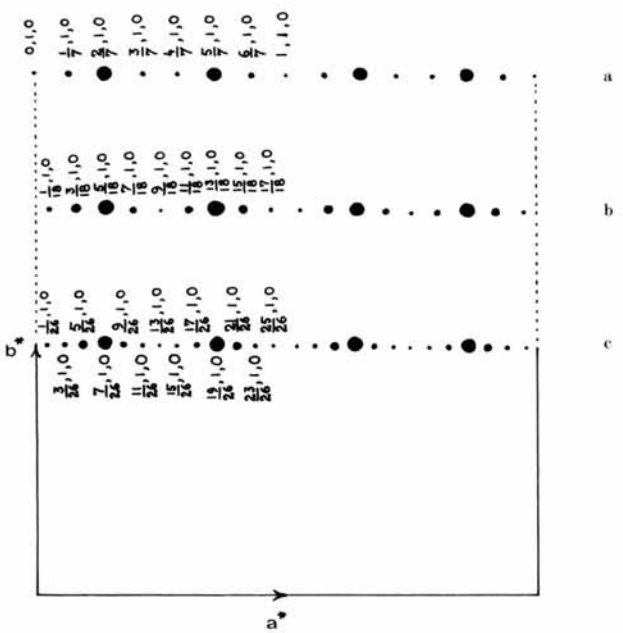

Fig. 8. The three reciprocal rows *a*, *b* and *c* of reflections $X10$ corresponding to the three diffraction patterns of Figs. 4, 5 and 6.

Model proposed for ordered Ag_3Mg

As it seems that we obtain ordinary long-period structures, *i.e.* with a long period along the **a** axis which is an integral multiple of **a**, we have tried to build periodic stackings of $L1_2$ units $\{\mathbf{a},\mathbf{b},\mathbf{c}\}$ along **a** (Fig. 9*a*) some of these units being shifted by $(\mathbf{b} + \mathbf{c})/2$ (Fig. 9*b*) with respect to the first unit. These units are identical to those chosen by Fujiwara (1957). The geometrical structure factor of the right cell in Fig. 9 will be affected by a phase factor $\exp\{2\pi i[(k + l)/2]\}$ with respect to the left cell, due to the antiphase vector, which turns out to be ± 1 along the row of spots $X10$, so that the stacking along **a** can be represented as a sequence of $+1$ and -1. This is similar to Zhdanov's notation for close-packed structures. For instance, the DO_{23} structure will be denoted $\bar{1}\bar{1}11$ or, more simply,

$\bar{2}2$: from left to right we first encounter two negative units ($\bar{2}$), then two positive units (2). Of course, it is immaterial if we begin with a negative unit or with a positive one: $2\bar{2}$ describes exactly the same structure.

Assuming kinematic theory (as usual), and the factor $(f_{Mg} - f_{Ag})$ being factorized for normalization, even a crude evaluation of the intensities of spots $X10$ eliminates a great number of *a priori* possible models by using the known properties of the Patterson function. The Patterson, or self-correlation function, *i.e.* the Fourier transform of intensities $I(h_j,k_j,l_j)$

$$P(x,y,z) = \sum_j I(h_jk_jl_j) \exp[2\pi i(h_j x + k_j y + l_j z)],$$

gives information on the first, second, third *etc.* neighbours. Here we are interested in the self-correlation of N $L1_2$ cells along the **a** direction. So we consider

$$P(x,0,0) = \sum I(X10) \exp\{2\pi i x X\}, \quad (0 \le x \le N-1).$$

Also, we know *a priori* that normalized $P(0,0,0)$ = sum of the products $(+1)(+1)$ and $(-1)(-1)$ and thus: $P(0,0,0) = N$.

Let us take for instance the case of the pattern of Fig. 4. The period is 7**a** so that $N = 7$. We measure approximately the intensities of the $X10$ spots by the square of the spot diameters, and find:

$X10$:	010	$\frac{1}{7}10$	$\frac{2}{7}10$	$\frac{3}{7}10$	$\frac{4}{7}10$	$\frac{5}{7}10$	$\frac{6}{7}10$
intensities:	1	3	18	2	2	18	3

We obtain:

$P(0,0,0) = 47$ (= the sum of all intensities without the exp factor)

$$P(1,0,0) = 1 + 3\exp\frac{2\pi i}{7} + 18\exp\frac{4\pi i}{7} + 2\exp\frac{6\pi i}{7} + 2\exp\frac{8\pi i}{7} + 18\exp\frac{10\pi i}{7} + 3\exp\frac{12\pi i}{7} = -6{\cdot}87.$$

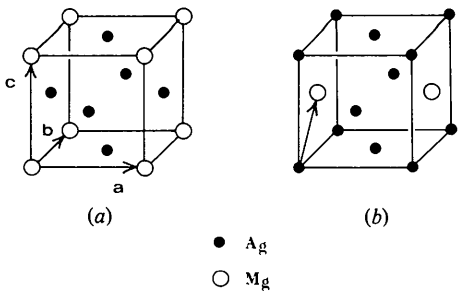

Fig. 9. (*a*) Unit cell of positive type (denoted: 1). (*b*) Unit cell of negative type (denoted: $\bar{1}$): antiphase vector: (**b** + **c**)/2.

But as $N = 7$, we can normalize $P(0,0,0)$ to 7. All values of the Patterson function must be odd integers because N is odd: $(f_{Mg} - f_{Ag})$ being factorized, we have a sum of N products each of them being -1 or $+1$, and after cancellation of an obviously even number of them, the result is odd. With $P(0,0,0) = 7$, we obtain for $P(1,0,0)$:

$$P(1,0,0) = -1{\cdot}02 \sim -1.$$

This means that among seven first neighbours, we obtain an excess of one dissimilar first neighbour, *i.e.* we have three similar first neighbours and four dissimilar first neighbours.

After the same calculation and normalization on $P(2,0,0)$, we obtain:

$$P(2,0,0) = -4{\cdot}51 \sim -5.$$

We thus have only one similar second neighbour and six dissimilar second neighbours.

In the instance considered, the knowledge of $P(1,0,0)$ and of $P(2,0,0)$ is sufficient: the structure is $11\bar{1}11\bar{1}\bar{1}$, or in Zhdanov's notation: $2\bar{2}2\bar{1}$. No other structure with a length of 7 is possible. Note that we have not used the fact that $1{\cdot}6 \le \bar{M} \le 2$. For $\bar{M}$ we find:

$$\bar{M} = \frac{3 \times 2 + 1}{4} = \frac{7}{4} = 1{\cdot}75.$$

The smallest distance between visible spots $X10$ will correspond to the 'fundamental' (= largest) interfringe seen when imaging through an objective aperture: the parameter of the disordered cell being about 4 Å, we get for the $2\bar{2}2\bar{1}$ structure $4 \times 7 = 28$ Å, which is actually observed (Fig. 7).

For the structure corresponding to Fig. 5, the total number of units stacked along **a** is 18. But as the Bravais lattice is I we must first have a certain arrangement of 9 $L1_2$ units and then the symmetrical arrangement $\bar{9}$. Here we find the arrangement $2\bar{2}2\bar{1}2\bar{2}2\bar{1}$, with $\bar{M} = \frac{18}{10} = 1{\cdot}80$. Other structures are eliminated by comparison of calculated $\bar{M}$ with measured $\bar{M}$.

For the structure corresponding to Fig. 6, the same reasoning leads to an I Bravais lattice and an arrangement $2\bar{2}2\bar{2}2\bar{1}2\bar{2}2\bar{2}2\bar{1}$ with $M = \frac{26}{14} = 1{\cdot}86$.

Our results are collected in Table 1. The kinematic intensities calculated from these models, in units of $(f_{Mg} - f_{Ag})$, are collected in Table 2 for spots $X10$, and are in good agreement with observed intensities. We have recently obtained high-resolution images of structures $\bar{M} = \frac{7}{4}$ and $M = \frac{18}{10}$, which definitely prove the correctness of our model. These images will be published in this journal in a subsequent paper.

The two diffraction patterns already published by Hanhi, Mäki & Paalassalo (1971) correspond to $\bar{M} = \frac{18}{10}$ for their Fig. 3 and $\bar{M} = \frac{26}{14}$ for their Fig. 5. Of course, their patterns show the three equivalent orientation domains.

Table 1. *Structures of the different ordered* Ag_3Mg *phases*

Structures (Zhdanov's symbol)	Length (in units of a)	$\bar{M}$	Remarks
$2\bar{2}1\bar{2}2\bar{1}$	10	$\frac{10}{6}=\frac{5}{3}=1{\cdot}67$	Observed (Vanderschaeve, 1978) *I*4/*mmm*
$2\bar{2}2\bar{1}$	7	$\frac{7}{4}=1{\cdot}75$	Observed (Fig. 4) 25 at.% Mg *P*4/*mmm* Largest interfringe = 28 Å (Fig. 7)
$2\bar{2}2\bar{2}1\bar{2}2\bar{2}2\bar{1}$	18	$\frac{18}{80}=\frac{9}{5}=1{\cdot}80$	Observed (Fig. 5) 24 at.% Mg *I*4/*mmm*
$2\bar{2}2\bar{2}2\bar{1}$	11	$\frac{11}{6}=1{\cdot}83$	Not observed *P*4/*mmm*
$2\bar{2}2\bar{2}2\bar{1}2\bar{2}2\bar{2}2\bar{1}$	26	$\frac{26}{14}=\frac{13}{7}=1{\cdot}86$	Observed (Fig. 6) 23·5 at.% Mg *I*4/*mmm* Largest interfringe = 52 Å (Fig. 8 in paper by Hahni, Mäki & Paalassalo, 1971)
$2\bar{2}$	4	2	Observed (Fig. 3) 22 at.% Mg *I*4/*mmm* (DO_{23})

Table 2. *Calculated intensities for the three models corresponding to* $\bar{M}=\frac{7}{4}$, $\bar{M}=\frac{9}{5}$, *and* $\bar{M}=\frac{13}{7}$ *for spots* $X10$

25 at.% Mg $\bar{M}=\frac{7}{4}$		24 at.% Mg $\bar{M}=\frac{9}{5}$		23·5 at.% Mg $\bar{M}=\frac{13}{7}$	
X, 1, 0	Intensities	X, 1, 0	Intensities	X, 1, 0	Intensities
$\frac{1}{7}$, 1, 0	2·6	$\frac{1}{18}$, 1, 0	5	$\frac{1}{26}$, 1, 0	4·2
$\frac{2}{7}$, 1, 0	20	$\frac{3}{18}$, 1, 0	16	$\frac{3}{26}$, 1, 0	7
$\frac{3}{7}$, 1, 0	1·2	$\frac{5}{18}$, 1, 0	132	$\frac{5}{26}$, 1, 0	32
$\frac{4}{7}$, 1, 0	1·2	$\frac{7}{18}$, 1, 0	7	$\frac{7}{26}$, 1, 0	275
$\frac{5}{7}$, 1. 0	20	$\frac{9}{18}$, 1, 0	4	$\frac{9}{26}$, 1, 0	12
$\frac{6}{7}$, 1, 0	2·6	$\frac{11}{18}$, 1, 0	7	$\frac{11}{26}$, 1, 0	5
$\frac{7}{7}$, 1, 0	1	$\frac{13}{18}$, 1, 0	132	$\frac{13}{26}$, 1, 0	4
		$\frac{15}{18}$, 1, 0	16	$\frac{15}{26}$, 1, 0	5
		$\frac{17}{18}$, 1, 0	5	$\frac{17}{26}$, 1, 0	12
				$\frac{19}{26}$, 1, 0	275
				$\frac{21}{26}$, 1, 0	32
				$\frac{23}{26}$, 1, 0	7
				$\frac{25}{26}$, 1, 0	4·2

Vanderschaeve (1978) has communicated to us a photograph of a diffraction pattern of the structure $2\bar{2}1\bar{2}2\bar{1}$ with $\bar{M}=\frac{10}{6}=1{\cdot}67$. It comes from a 26·5 at.% Mg sample annealed at 370°C for 4 d.

As the Mg concentration decreases, there is an increasing proportion of cells of type 2, and the long period increases more and more until finally the cells of type 1 completely disappear and we are left with only $2\bar{2}$ (DO_{23}) for compositions of about 22 at.% Mg.

Conclusions

Contrary to the case of standard PAP structures, such as AuCu, Au_3Cu, Cu_3Pd, *etc.*, the Ag_3Mg alloy shows a discontinuous series of long-period ordered phases, stable in small concentration ranges, the latter becoming smaller and smaller as we approach concentrations corresponding to $M=2$ (about 22 at.% Mg).

The fact that no $L1_2$ phase seems to exist in Ag_3Mg may well be correlated to the fact that it is not a PAP structure, and so our criticism of Sato & Toth's theory is still valid (Guymont & Gratias, 1976).

Finally, the term PAP could be reserved for structures which exhibit those characteristic features discussed in the *Introduction*. With this convention, ordered Ag_3Mg would no longer be described as a PAP structure, and would be placed among these regular long-period structures whose long period depends on composition, as is the case for Magnéli or Wadsley phases such as niobium oxides (see *e.g.* Iijima, Kimura & Goto, 1974) or perovskite-like compounds (see *e.g.* Portier, Carpy, Fayard & Galy, 1975).

We are indebted to Professor P. Pério for a number of corrections and many useful discussions.

References

FUJIWARA, K. (1957). *J. Phys. Soc. Jpn*, **12**, 7–13.

FUJIWARA, K., HIRABAYASHI, M., WATANABE, D. & OGAWA, S. (1958). *J. Phys. Soc. Jpn*, **13**, 167–174.

GANGULEE, A. & BEVER, B. (1968). *Trans. Metall. Soc. AIME*, **242**, 278–283.

GLOSSOP, A. B. & PASHLEY, D. W. (1959). *Proc. Roy. Soc. London Ser. A*, **250**, 132–146.

GRATIAS, D., CONDAT, M. & FAYARD, M. (1972). *Phys. Status Solidi A*, **14**, 123–128.

GUYMONT, M. & GRATIAS, D. (1976). *Phys. Status Solidi A*, **36**, 329–334.

HAHNI, K., MÄKI, J. & PAALASSALO, P. (1971). *Acta Metall.* **19**, 15–20.

IIJIMA, S., KIMURA, S. & GOTO, M. (1974). *Acta Cryst.* A**30**, 251–257.

JEHANNO, G. (1965). *Structures à Longues Périodes dans les Alliages Or–Cuivre*, Thesis. Report CEA R2812, Univ. of Orsay.

JEHANNO, G. & PÉRIO, P. (1964). *J. Phys.* **25**, 966–974.

JOHANNSON, C. H. & LINDE, J. O. (1936). *Ann. Phys.* **25**, 1–48.

OGAWA, S., IWASAKI, H. & TERADA, A. (1973). *J. Phys. Soc. Jpn*, **34**, 384–390.

OGAWA, S., WATANABE, D., WATANABE, H. & KOMODA, T. (1958). *Acta Cryst.* **11**, 872–875.

PÉRIO, P. & TOURNARIE, M. (1959*a*). *Acta Cryst.* **12**, 1032–1038.

PÉRIO, P. & TOURNARIE, M. (1959*b*). *Acta Cryst.* **12**, 1044–1047.

PIANELLI, A. (1959). *C. R. Acad. Sci.* **248**, 2475–2476.

PORTIER, R., CARPY, A., FAYARD, M. & GALY, J. (1975). *Phys. Status Solidi A*, **30**, 683–697.
SATO, H. & TOTH, R. S. (1965). *Alloying Behaviour and Effects in Concentrated Solid Solutions*, pp. 295–419. New-York: Gordon & Breach.
SCHUBERT, K., KIEFER, B., WILKENS, M. & HAUFLER, R. (1955). *Z. Metallkd.* **46**, 692–715.
VANDERSCHAEVE, G. (1969). *Phys. Status Solidi*, **36**, 103–117.
VANDERSCHAEVE, G. (1978). Private communication.

Acta Cryst. (1979). A**35**, 188–193

Mögliche Kristallstrukturen für oktaedrische Moleküle MX_6 bei dichtester Packung der X-Atome

VON ULRICH MÜLLER

Fachbereich Chemie der Universität Marburg, Lahnberge, D-3550 Marburg, Bundesrepublik Deutschland

(*Eingegangen am* 23. *Februar* 1978; *angenommen am* 8. *August* 1978)

Abstract

As long as there is no thermally induced disorder, octahedral MX_6 molecules crystallize with a close-packed arrangement of X atoms in which one sixth of the octahedral holes are occupied by M atoms. On consideration of the symmetry restrictions imposed by the partial occupation of the octahedral holes, the possible space groups and structures are deduced with the aid of group–subgroup relationships. Centrosymmetric space groups that can be achieved include: (1) all trigonal, rhombohedral and monoclinic space groups, *Pnmn*, *Pnma*, *Pnab* and $P\bar{1}$ for hexagonal close packing of the X atoms; (2) *Pcmn* and *Pcab* for the double-hexagonal close packing; (3) *Fddd*, *Bbmb*, all monoclinic space groups and $P\bar{1}$ for cubic close packing. The most important molecular arrangements are illustrated and their expected cell dimensions are given. The known structures of WCl_6, UCl_6 and numerous hexafluorides correspond to some of the predicted possibilities.

Das von Bärnighausen (1975) entwickelte Konzept zur systematischen Beschreibung von Kristallstrukturverwandtschaften mit Hilfe der kristallographischen Gruppe–Untergruppe-Beziehungen (Billiet, Sayari & Zarrouk, 1978; Neubüser & Wondratschek, 1966, 1969) kann auch dazu herangezogen werden, um vorauszusagen, welche Raumgruppen möglich sind, wenn eine gegebene Verbindung unter Einhaltung bestimmter Randbedingungen kristallisieren soll. Für die möglichen Raumgruppen lassen sich Strukturmodelle angeben und Erwartungswerte für die Gitterkonstanten berechnen. Sind von einer Verbindung die Gitterkonstanten bekannt, so kann durch Vergleich mit den Erwartungswerten ihre wahrscheinliche Kristallstruktur vorausgesagt werden. In einer vorangegangenen Arbeit (Müller, 1978*a*) waren so Strukturmöglichkeiten für dimere Pentahalogenide abgeleitet worden. Nachfolgend werden analoge Überlegungen für die Kristallstrukturen oktaedrischer Molekülverbindungen MX_6 angestellt.

Randbedingungen

Es sei vorausgesetzt, dass MX_6-Moleküle unter Einhaltung der folgenden Randbedingungen kristallisieren:

(1) Die X-Atome sollen eine hexagonal-, doppelthexagonal- oder kubisch-dichteste Kugelpackung annehmen.

(2) Ein Sechstel der Oktaederlücken dieser Packung soll durch M-Atome besetzt werden.

(3) Damit ein Molekülgitter entsteht, müssen die Lücken aller Nachbaroktaeder um ein besetztes Oktaeder frei bleiben.

(4) Die Betrachtung sei auf zentrosymmetrische Raumgruppen beschränkt. Diese Einschränkung wird durch die Erfahrung gerechtfertigt, dass zentrosymmetrische Moleküle nur in seltenen Ausnahmefällen in nicht-zentrosymmetrischen Raumgruppen kristallisieren (die bekannten Ausnahmefälle beschränken sich ausserdem auf Moleküle der Punktsymmetrie $2/m$; Müller, 1978*b*).

Die Randbedingungen lassen für die Moleküle nur bestimmte Orientierungsmöglichkeiten zu und bedingen, dass bestimmte Symmetrieelemente der Kugelpackung verloren gehen. Die realisierbaren Raumgruppen ergeben sich dann, wenn man von allen Untergruppen der Kugelpackungsraumgruppe diejenigen streicht, welche nicht erhaltbare Symmetrieelemente besitzen.

0567-7394/79/010188-06$01.00